Applied Geochemistry 111 (2019) 104445

Contents lists available at ScienceDirect

Applied Geochemistry

journal homepage: http://www.elsevier.com/locate/apgeochem

Rapid water-rock interactions evidenced by hydrochemical evolution of flowback fluid during hydraulic stimulation of a deep geothermal borehole in granodiorite: Pohang, Korea

Neil M. Burnside [a,*], Rob Westaway [a], David Banks [a], Günter Zimmermann [b], Hannes Hofmann [b], Adrian J. Boyce [c]

[a] School of Engineering, University of Glasgow, James Watt Building South, Glasgow, G12 8QQ, UK
[b] Deutsches GeoForschungsZentrum (GFZ), Telegrafenberg, 14473, Potsdam, Germany
[c] Scottish Universities Environmental Research Centre, East Kilbride, G75 0QF, UK

ARTICLE INFO

Editorial handling by Dr D. Wolff-Boenisch

Keywords:
Geothermal
Pohang
Hydrology
Geochemistry
Stimulation
Isotope

ABSTRACT

Flowback water from the 4215 m deep (True Vertical Depth) PX-1 borehole, following the August 2017 hydraulic stimulation of a granodiorite geothermal reservoir in Pohang, South Korea, was monitored for a suite of physicochemical, chemical and isotopic parameters. The results provide unique insights into mixing processes, fluid evolution and rapid water-rock interaction in a deep geothermal system. Injected water for stimulation was relatively fresh, oxidising surface water, with temperature 29.5 °C and pH c. 6.5. The flowback water showed an increasing content of most solutes, with the evolution conforming to an exponential 'flushing' model for conservative solutes such as chloride. Flowback water became progressively Na–Cl dominated, with a circumneutral pH (7.1) and negative oxidation-reduction potential (c. −180 mV). Some solutes (including, Na, K and Si) increased more rapidly than a flushing model would suggest, implying that these had been acquired by the flowback water due to mineral hydrolysis. Stable isotopes of O and H indicate that initially meteoric waters have undergone geothermal oxygen isotope exchange with minerals. Evolution of redox species in recovered water suggests progressively oxidising zonation around the injection borehole in an otherwise reducing reservoir. Rapidly increasing silica concentrations in flowback water suggests extensive quartz dissolution and indicated a reservoir temperature of up to 169 °C. This lends plausible, if equivocal support to the hypothesis that quartz dissolution by injection water may have contributed to triggering movement on the pre-stressed fault associated with the November 2017 Mw 5.5 Pohang earthquake.

1. Introduction

The Pohang geothermal site (129°22′46.08″E, 36°06′23.34″N) is located 1.5 km north of the city of Pohang, on the east coast of the Korean Peninsula. Pohang experiences a humid subtropical climate (Figure A1), with an annual average precipitation (1961–76) of 1106 (±250) mm and an annual average air temperature of 13.1 (±0.5) °C (IAEA/WMO, 2018). For the more recent period of 1981–2010, slightly higher values of 1152 mm and 14.2 °C are cited by KMA (2016). The bulk of the precipitation falls between July and September, as a result of the East Asian summer monsoon. The monthly average air temperature reaches as low as +1–2 °C in January, but as high as 25 °C in summer (when the trials described in this paper were carried out).

The geothermal project comprises two deep boreholes to depths of c. 4.3 km in a Permian granodiorite (quartz, plagioclase, microcline, hornblende, biotite; Lee et al., 2011) with mafic gabbro and amphibolite dykes (Kim et al., 2018; Lee et al., 2014). The site was intended to be operated as an Enhanced Geothermal System (EGS), with one borehole used for production of hot fluid and the second being used for reinjection. Several cycles of hydraulic stimulation have been applied in an attempt to improve the natural injectivity and productivity and to establish hydraulic connectivity between the boreholes (Park et al., 2017).

The exploration of the Heunghae Basin (Park et al., 2015) commenced in 2010, whereas the first borehole, PX-1, was drilled in 2012–13 (initially as a vertical borehole) and then side-tracked in 2016.

* Corresponding author.
E-mail address: neil.burnside@glasgow.ac.uk (N.M. Burnside).

https://doi.org/10.1016/j.apgeochem.2019.104445
Received 1 August 2019; Received in revised form 9 October 2019; Accepted 16 October 2019
Available online 18 October 2019

It was completed as a deviated borehole (deviated c. 600 m to the WNW with a measured depth of 4362 m) to a true vertical depth (TVD) of 4215 m (Yoon et al., 2015; Hofmann et al., 2019). The lowermost open hole section is 313 m long and 8 ½" in diameter (Hofmann et al., 2019). The total volume of PX-1 borehole is calculated as 85 m^3, with 74 m^3 in the cased portion and 11 m^3 in the lowest (open hole granodiorite) section (Banks et al., 2019). The vertical well PX-2 was drilled and completed in 2015 down to 4348 m, with lowermost 140 m open hole section at 8 ½" diameter (Hofmann et al., 2019). The Pohang granodiorite is encountered in the boreholes at a depth of around 2300 m, and is overlain by a succession of Cretaceous and Tertiary tuffs and sedimentary rocks (sandstones, siltstones and mudstones), with a surface cover of Quaternary alluvium. The granodiorites have been dated to 268 ± 4 Ma (Lee et al., 2015). Geothermal gradients of 31–38 °C/km have been recorded in the Mesozoic sequence overlying the granodiorites and temperatures in excess of 90 °C have been recorded at 2000 m depth (Lee et al., 2015), and 103 °C at 2250 m depth (Yoon et al., 2015) (i.e. just above the top of the Pohang granodiorite). Based on geothermal gradients, a temperature of 160 °C has been calculated at 4.3 km depth (Kim and Lee, 2007).

Stimulation has typically been applied as a series of short-term cyclic injections of surface water or shallow groundwater. During the initial stimulation of PX-2 in January–February 2016, maximum wellhead pressures of 89.2 MPa and flow rates of 46.8 kg/s were reportedly applied to the bottom 140 m open section of PX-2, as daily episodes comprising several shorter scale cycles (Park et al., 2017).

Subsequent hydraulic stimulation was carried out in PX-1 in December 2016–January 2017, PX-2 in April 2017, PX-1 in August 2017 and PX-2 in September 2017 (Kim et al., 2018; Lee, 2017; Westaway and Burnside, 2019). In total, over the five stimulation episodes (January 2016–September 2017), 5663 m^3 water was injected to PX-1 and 7135 m^3 to PX-2 (12,798 m^3 total), while totals of 3968 m^3 and 2989 m^3 (6957 m^3 combined) were recovered as flowback from PX-1 and PX-2, respectively. Thus, a total unrecovered volume of 5841 m^3 remains in the subsurface (1695 m^3 in PX-1 and 4146 m^3 in PX-2) (Lee et al., 2019).

This paper will focus on the sampling of injection water and subsequent post-stimulation flowback after the August 2017 stimulation of PX-1. It should be noted that, in November 2017, a major M_w 5.5 earthquake occurred in the near vicinity of the EGS project There has been significant speculation regarding whether the hydraulic stimulation activities may have been responsible for triggering that earthquake (Kim et al., 2018; Westaway and Burnside, 2019; Grigoli et al., 2018; Zastrow, 2019; Lee et al., 2019). An expert panel, appointed by the Republic of Korea government, has reported on this topic and concluded that "*small earthquakes induced by high-pressure injection into the PX-2 well activated the fault that ultimately ruptured in the MW 5.5 earthquake*" (Lee et al., 2019). As our study investigates water-rock interaction in the near-PX-1 well environment, we are unable to comment on the architecture or the chemical composition of rock within, or immediately proximal to, the slipped fault. However, this paper is the most comprehensive hydrochemical data set available for the Pohang site, so it provides essential information for any assessment of hydrochemical changes as a potential implicating factor in that event.

1.1. Previous hydrochemical work on Pohang thermal granitic waters

Thermal groundwater resources in Korea are often associated with granite outcrops or subcrops, and are characterised as alkaline (pH = 8–9.5), of low total dissolved solids, fluoride-rich (5–15 mg/L) and of Na–HCO_3 type (Yum, 1999). There is a thermal spring resort at Pohang (129° 19′ 59.8″ E 36° 05′ 06.2″ N), which utilises 44 °C water derived from a borehole, open to the Pohang granite at 600–700 m beneath its Tertiary cover. The reported pumped yield from the thermal borehole is 1000 m^3/d (11.6 L/s on average) and the water is of Na–HCO_3 type (Lee et al., 2011). Table 1 shows the composition of the water as of 2009.

1.2. Previous hydrochemical work on Pohang geothermal site

As already noted, up to August 2017, a total of three hydraulic stimulations, one in PX-1 and two in PX-2, had taken place at the Pohang site. However, only very limited hydrochemical data have been produced from the flowback that occurred prior to August 2017. Four samples of flowback water were collected from the stimulation of PX-1 in December 2016–January 2017 (Banks and Brehme, 2017). The results from analysis of these samples are shown in Fig. 1. It is particularly noteworthy that silica (SiO_2) concentration rose dramatically during flowback, from 14 mg/L in the initial injection water up to 137 mg/Las SiO_2 after 14 h, which indicates a significant component of thermal water and reflects the high solubility of silica at elevated temperature (Rimstidt and Barnes, 1980). The following components also progressively increased in flowback water: Cl^-, Br^-, $SO_4^{=}$, Ba, Mo, Na, K, Fe and, to a lesser extent, Ca. Mg was the sole component showing a tendency to decline (Banks and Brehme, 2017). The Br^-/Cl^- molar ratio decreased during flowback from 0.00084 to 0.00065, relatively low values that suggest halite dissolution or intense evapoconcentration (Davis et al., 1998; Woods and Sandford, 2007).

2. Summary of hydraulic stimulation routines

The main water source for well stimulation was from the Namdong No.2 Reservoir, a 19,000 m^3 pond of surface water used for irrigation, c. 250 m NNE of the borehole site. Water was pumped from this reservoir at 40 L/s through a 12" diameter pipe, complete with a 3.5 × 1.5 cm oval slot filter. The surface water appeared visually clear but hosted abundant plant and animal life (including fish and tadpoles) and is likely to have contained small quantities of particulate or organic matter.

The site also possesses a shallow groundwater borehole, used to supply potable water to on-site buildings (and believed to have been used for preparing drilling mud). Although the vast majority of water used for hydraulic stimulation was surface water from the pond, it cannot be excluded that some of the water, in the earliest stages of stimulation, may have been derived from the groundwater borehole. For this reason, both water from the pond (3 samples from different parts of the pond, samples SK1-SK3) and from the groundwater borehole were sampled (sample SK4).

For the August 2017 stimulation, water was pumped from the pond, without any treatment or chlorination, to a storage tank, from which it was injected under pressure into well PX-1. For this stimulation, a 180 μm filter was installed between the initial pond water storage tanks and wellhead storage tanks. On 7th August, the injection water was sampled both before (SK21) and after (SK20) this filter.

Table 1
Groundwater composition (2009) from Pohang thermal spa borehole, after Lee et al. (2011).

Sample PDHS-09	Units	Value
Temperature	°C	44.0
pH	pH units	8.4
Electrical conductivity	μS/cm	1977
Total dissolved solids	mg/L	1150
Na	mg/L	536
Ca	mg/L	3.6
Mg	mg/L	1.65
K	mg/L	3.57
HCO_3^-	mg/L	992
Alkalinity	meq/L	16.25
Cl^-	mg/L	122
$SO_4^{=}$	mg/L	17.5
F^-	mg/L	4.58
Br^-	mg/L	<0.2
Sr	μg/L	222
Li	μg/L	230
SiO_2	mg/L	20.1
Br^-/Cl^- ratio	molar ratio	<0.00073

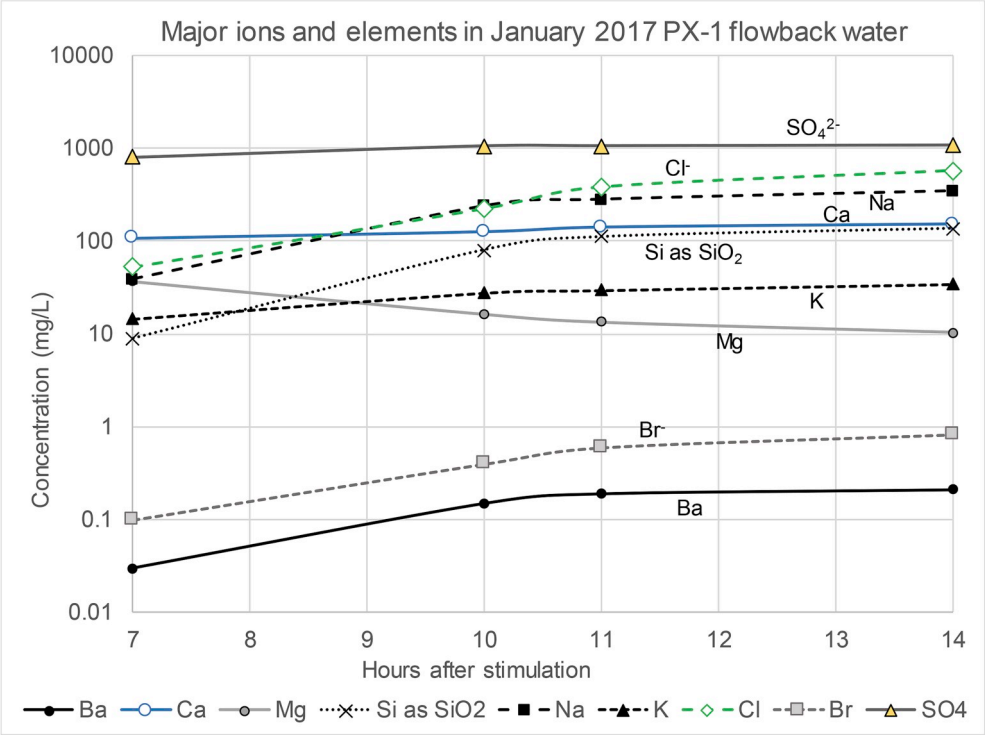

Fig. 1. Concentrations of ions (Cl^-, SO_4^{2-}, Br^-) and elements (Ba, Ca, Mg, Si, Na, K) in flowback water from borehole PX-1, as a function of time following cessation of injection and commencement of flowback in January 2017. Modified after (Banks and Brehme, 2017).

The August 2017 trial stimulation involved the cyclic injection of c. 1756 m^3 water to PX-1 between 7th and 14th August (Kim et al., 2018; Hofmann et al., 2019). This cyclic stimulation was carried out at rates of≤10 L/s and wellhead pressures of up to c. 23 MPa (Hofmann et al., 2019). Flowback following the injection (hydraulic stimulation) trials commenced at 09:34 on 14th August 2018 and the flowback water was collected in storage tanks and then removed for off-site disposal by tanker. During flowback, samples of water were collected at 2 to 3 hourly intervals until 15th August. Thereafter, sample frequency was reduced to 2 per day and thereafter to 1 per day. Flowback rates and cumulative flowback have been estimated as the flowback period progressed (Hofmann et al., 2019), with rates declining rapidly from over 6 L/s to around 0.6 L/s after c. 140 hrs flowback (Westaway and Burnside, 2019). In the period 16th-24th August, works were carried out on the wellhead and casing of the borehole. The inner casing of well PX-1 was cut at 800 m depth, to permit the installation of a submersible pump (Westaway and Burnside, 2019). No samples were collected in the period 21st - 24th August. Between 25th August and 1st September 2017, a production (pumping) test was carried out, using the submersible pump installed at c. 800 m depth, during which samples were also taken. Flowback and pumping following the August 2017 injections resulted in the total production of c. 1771 m^3 (Hofmann et al., 2019) water, slightly in excess of the quantity injected.

3. Methods

Two sets of samples of injection and flowback waters were collected during August 2017 PX-1 stimulation trials:

(1) Surface water used for injection (SK1-3 and SK20, 21) and groundwater from an on-site shallow borehole (SK4) in the period 3rd-7th August. In addition, a range of bulk samples (SK5-19) acquired by Korean staff from various previous air-lift and bleed-off events from PX-1 and PX-2 in the period Dec. 2016 to 3rd August 2017 were collected. These sample aliquots were prepared as follows (no acidification was carried out in the field):
   (a) 3 × 15 ml filtered (0.45 μm filter on hand-held syringe) aliquots in polypropylene screw capped flasks (ion chromatography; IC)
   (b) 1 × unfiltered 50 ml aliquot in polypropylene screw capped flasks (alkalinity)
   (c) 3 × unfiltered 10 ml aliquots in glass vials, sealed with parafilm (stable isotope analysis)
   (d) 3 × unfiltered 10 ml aliquots in glass vials (inductively coupled plasma optical emission spectrometry; ICP-OES). These samples were subsequently decanted at the University of Glasgow (UoG) into 50 ml sample flasks for analysis by Concept Life Sciences Analytical & Development Services Ltd (CLS).

(2) Flowback water (SK22-SK46) from the test simulation period. These samples were taken by site crew, using a cut-off plastic flask either from the point of entry of the discharge pipe to the flowback fluid tank (initially) or directly from the well head (later in the flowback period when temperatures had declined). Sampled water was transferred directly into either 2 × 500 mL or 1 × 1000 mL plastic flasks which were sealed (unfiltered and unacidified) and returned to UoG. Following the flowback period, bulk samples were collected during production testing (SK47-SK51, 25th August – 1st September) and from concurrent bleed-off of PX-2 (SK52-SK53, 27th-28th August) and dispatched to UoG. For samples collected following 1900 h on 16th August, the aforementioned casing modifications may have had some impact on PX-1 water chemistry (e.g. mixing of flowback with water previously trapped behind the inner casing). On arrival at UoG, these samples were used to prepare filtered and unfiltered sample aliquots as described in 1(a)-(d) above.

At the Pohang well site, field determinations of pH, temperature, electrical conductivity (EC) and oxidation-reduction potential (ORP)

were carried out on the flowback water using a Myron Ultrameter II 6PFC instrument (with results corrected to 25 °C), at the points where samples were collected. A separate set of temperature measurements were also made by members of the rig crew, who reported a typical range from 50 to 65 °C. Following the wellhead and flowback tank determinations, replicate determinations of pH and EC were carried out on sampled water at a site building using a Thermo Scientific Orion Star A329 portable meter. During the final production testing period (SK47-SK53), Ultrameter measurements were made upon delivery of samples to UoG.

One aliquot of each sample was used for a titration of total alkalinity (corresponding to bicarbonate concentration), using 0.16 or 1.6 M sulphuric acid, to a pH end-point of c. 4.5 (bromocresol green - methyl red indicator), with Hach Model 16900 digital titrator (Hach Company, Loveland, Colorado). UoG laboratory determinations follow the protocol of (Burnside et al., 2016). Anions and cations were measured using Dionex ICS-900 and ICS-1100 Ion Chromatography (IC) equipment. δ^2H and $\delta^{18}O$ stable isotopes were measured using VG Optima and Thermo Scientific Delta V isotope ratio mass spectrometers. Each collected aliquot (typically three per sample) was run in triplicate for isotope determination and values cited in this paper represent averages of those replicate determinations. ICP-OES (including dissolved silica, major, minor and trace metals, and major cations) was carried out on laboratory filtered and acidified aliquots by CLS, East Kilbride, UK (UKAS accreditation ISO/IEC 17025:2005).

3.1. Correspondence between analytical techniques and ion balance error

The two sets of analyses for Na^+, Ca^{++}, Mg^{++} by IC at UoG and by ICP-OES at CLS were well correlated, but the correlation for K^+ was somewhat poorer (Figure A2). In the remainder of this paper, the UoG IC data will be presented for Na^+, Mg^{++}, Ca^{++}, NH_4^+ and all anionic species, titration data will be utilised for alkalinity, and CLS data will be preferred for K^+ and presented for silica and other elements. An ion balance error was calculated for each of the 57 samples on the basis of major cations and anions. All samples had an ion balance error of within ±10% and 42 samples had an ion balance within ±5%, which is typically regarded as sufficiently accurate for groundwaters (Bartram and Balance, 1996; Misstear et al., 2017).

4. Results and discussion

Analytical results are presented in spreadsheet format in Appendix B.

4.1. Stable isotopes

Fig. 2a presents background H and O isotopic data compiled by IAEA and WMO (2018) for precipitation in the Pohang area. The weighted mean stable isotope contents of Pohang precipitation are -7.78 ± 0.88‰ for $\delta^{18}O$ and -50.9 ± 9.6‰ for δ^2H. Three local meteoric water line (LMWL) interpretations lie very slightly above the global line (GMWL). Summer precipitation at Pohang is typically more depleted in the heavy isotopes than the winter precipitation.

The groundwater from the shallow borehole lies close to the LMWL, at the isotopically depleted end of the range, possibly reflecting predominant summer groundwater recharge. The surface water (directly from the source pond and sampled during injection) lies a little below the LMWL at the isotopically enriched end of the range and could reflect evaporative processes during atmospheric exposure. PX-1 and PX-2 flowback water ranges from close to significantly below/right of the LMWL and water produced (airlifted) from PX-1 plots further below the GMWL (Fig. 2b). This suggests a component of deep granitic groundwater that has been substantially modified by water rock interaction. This is compatible with a rightwards oxygen-shift caused by water-rock isotopic oxygen exchange at temperatures in excess of 150 °C (Blattner, 1985; Clayton and Steiner, 1975). This effect is especially clear from the August 2017 flowback and production test data in Fig. 2b, where the composition evolves during flowback from the injected water composition to a more isotopically depleted signature lying to the right of the LMWL and GMWL.

4.2. Trends in physico-chemical parameters and water chemistry

Evolution of physico-chemical and ionic parameters throughout the

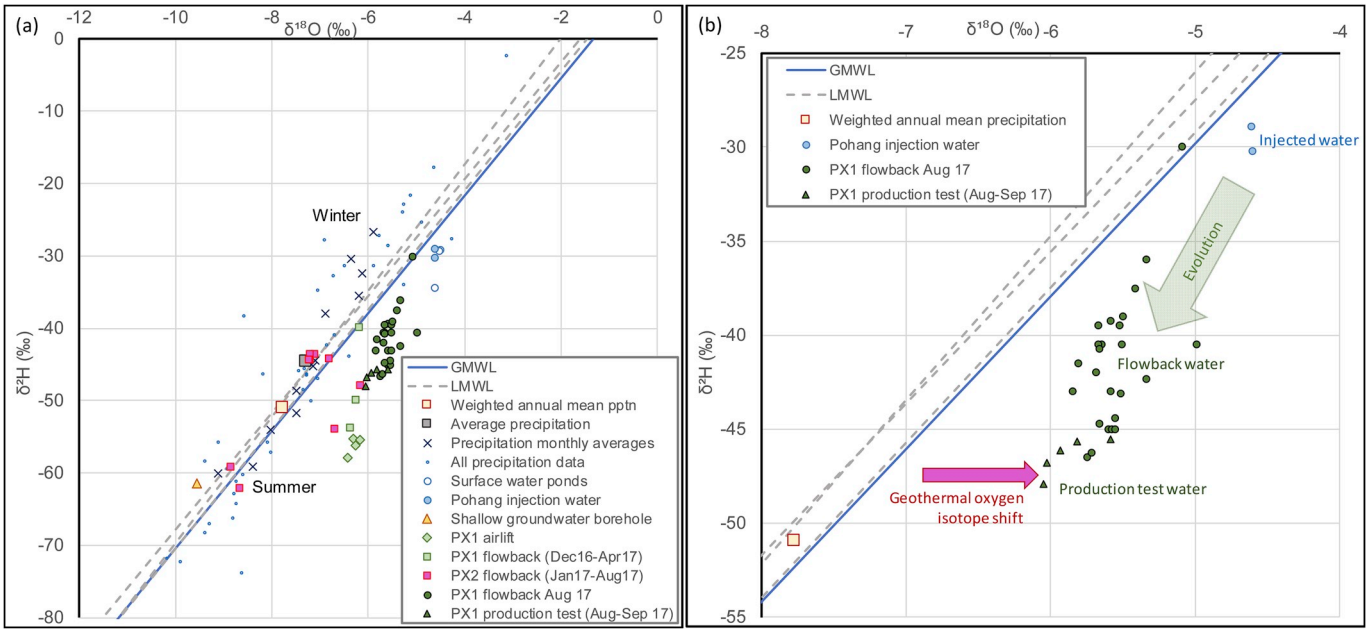

Fig. 2. Stable isotope results for surface water (pond), shallow groundwater (on-site borehole), injection water (derived from surface water pond) and fluid recovered from PX-1 and PX-2 at Pohang. These are compared with Pohang precipitation (actual monthly data points, monthly means, annual mean and weighted annual mean; IAEA/WMO, 2018), three possible local meteoric water line (LMWL) regressions (IAEA/WMO, 2018) and the global meteoric water line (GMWL). (b) Expanded view of (a) showing only injected water, weighted annual mean precipitation and flowback/production test data from PX-1 in August–September 2017.

flowback and production period are demonstrated by Figs. 3 and 4. Injected surface water was measured (on site) with a temperature of 29.5 °C, an EC (corrected to 25 °C) of 990–1300 μS/cm, an oxidising ORP of +160 to +190 mV, dissolved oxygen saturation of around 76–87% (pond samples SK1-SK3) and a sub-neutral pH of c. 6.5. It is of Ca–$SO_4^{=}$ type, with high ammonium (c. 6 mg/L) and potassium (c. 15 mg/L) that suggest presence of leachate from agricultural fertiliser (Fig. 4). A single post-filter sample from the injection line (SK20) demonstrated elevated pH (7.4) and sodium and chloride concentrations (120 and 163 mg/L, respectively) in relation to other surface water samples (SK21, SK1-SK3). Such variation might result from inadequate flushing of the storage tanks.

The variation in temperature and conductivity in the recovered water is shown in Fig. 3, as is the calculated cumulative quantity of flowback, which also allowed the rate of flowback to be estimated. Taking the estimated PX-1 volume of 85 m^3; the first two measurements (SK22 and SK23, at 0.35 h and 1.60 h, corresponding to 8.3 and 37.2 m^3 cumulative flowback), represent water that did not leave the borehole. As a result, these initial water samples closely resemble the injected water. Initial return samples have a pH of c. 7.6 which decreases to circumneutral values (average 7.09, standard deviation 0.18 for all flowback samples), after around 12 h flowback.

The rig crew temperature measurements are systematically higher than those by the UoG team, due to proximity of their measurement to the well head and the cooling that took place in the small (1.2 cm^3) measurement cell of the Ultrameter, and the rig crew determinations (where available) are preferentially cited here. The produced water initially has a temperature almost identical to the injected water (first two samples). With time this increases to a maximum of 64–65 °C after an elapsed time of 22–75 h. As the flowback rate sharply declines, flowback water temperature also declines to 47 °C, reflecting a slower ascent and greater thermal re-equilibration with cooler near-surface rocks.

Flowback water EC is initially a little higher than the injection water, but then falls back down to a level comparable to the injected water. It then starts to climb, roughly in proportion to the logarithm of time. The shape of the curve, with a quasi-log-linear central section and then a tendency to approach a limiting value, is reminiscent of an exponential 'flushed mixing tank' curve (Gzyl and Banks, 2007), where relatively fresh injected water is being flushed out of the borehole by a more brackish *in situ* groundwater. This *in situ* groundwater composition is presumed to represent a natural brackish formation water, partially influenced by previous episodes of freshwater injection. An exponential decay curve can be fitted to the EC data of the form

$$C = C_c - (C_c - C_0) \times e^{mx} \quad (1)$$

where x is a parameter used to quantify the flowback (time in Fig. 3 and volume in Fig. 7), C is concentration or EC, C_c and C_0 are the ceiling and initial values of C, and m is a decay constant (hr^{-1} or m^{-3} depending on x). In the case of EC versus time, the best fit parameterisation is $C_0 = 1380$ μS/cm, $C_c = 3250$ μS/cm, decay constant $= -0.02746$ hr^{-1}. In other words, the EC tends, with time, towards a value of 3250 μS/cm.

The flushing model is supported by trends in major solute concentrations. Increases in sodium and chloride are initially rapid before becoming less steep with time, in identical fashion to EC (Fig. 5a). In terms of meq/L, sodium exceeds calcium as the dominant cation after c. 4 h and chloride exceeds sulphate as the dominant anion after c. 17 h. Fig. 4d shows the water composition at 13.30 h on 14th August (3.9 h elapsed time). Concentrations of sodium and chloride eventually exceed 600 mg/L and 1000 mg/L by the latest production testing stage. Calcium and sulphate follow a similar, but less dramatic trend before levelling off to relatively stable values (180–200 mg/L and 500–520 mg/L, respectively) after c. 96 h (Fig. 5a). Potassium behaves similarly to calcium, but with a less pronounced increase in concentrations (15–36 mg/L). Alkalinity in the flowback fluid shows little variation: a slight peak after around 15–27 h at around 2.6 meq/L, followed by a modest decline to c. 1.4 meq/L by the end of production testing.

Magnesium is the one major element with a contrary trend (Fig. 5b). Concentrations decline sharply from c. 30 mg/L after commencement of flowback (c. 36 mg/L in injection water) in a quasi-exponential manner, and continue to fall to extremely low concentrations of only 1.5 mg/L in the last samples. Low magnesium concentrations are characteristic of many geothermal waters (Gendenjamts, 2003; Gunnlaugsson et al., 2014), due to the tendency of magnesium to be either precipitated as magnesium silicate minerals or be incorporated into the structure of secondary clays and sheet silicates (Gunnlaugsson et al., 2014; Cox and

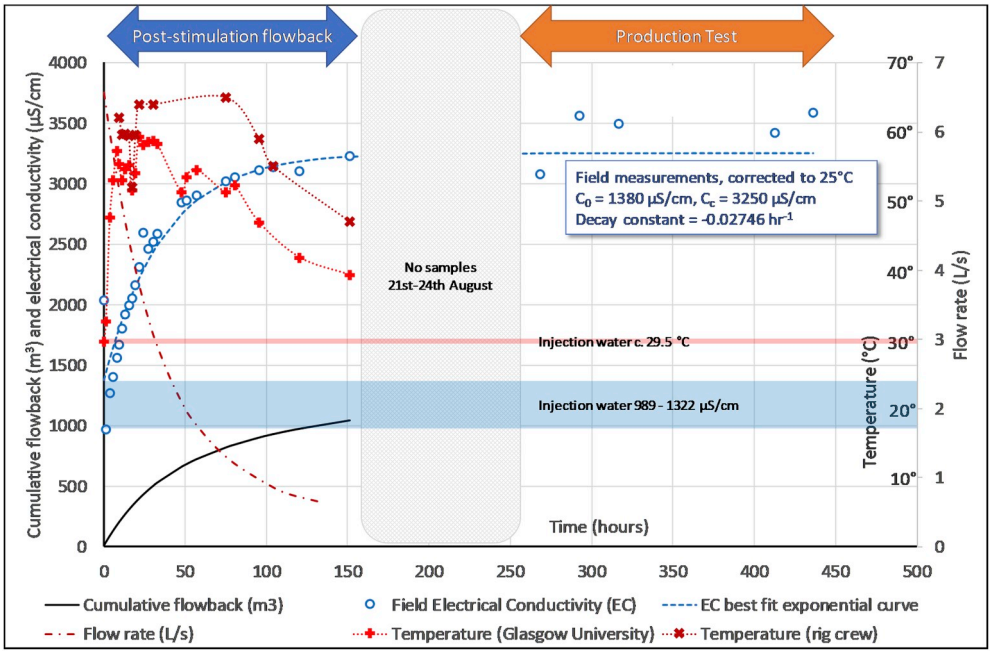

Fig. 3. Field-determined electrical conductivity and temperature in flowback fluid from PX-1, and water produced during production test of PX-1 in August 2017. Elapsed time is measured in hours since start of flowback, following hydraulic stimulation (09:34 on 14th August 2017).

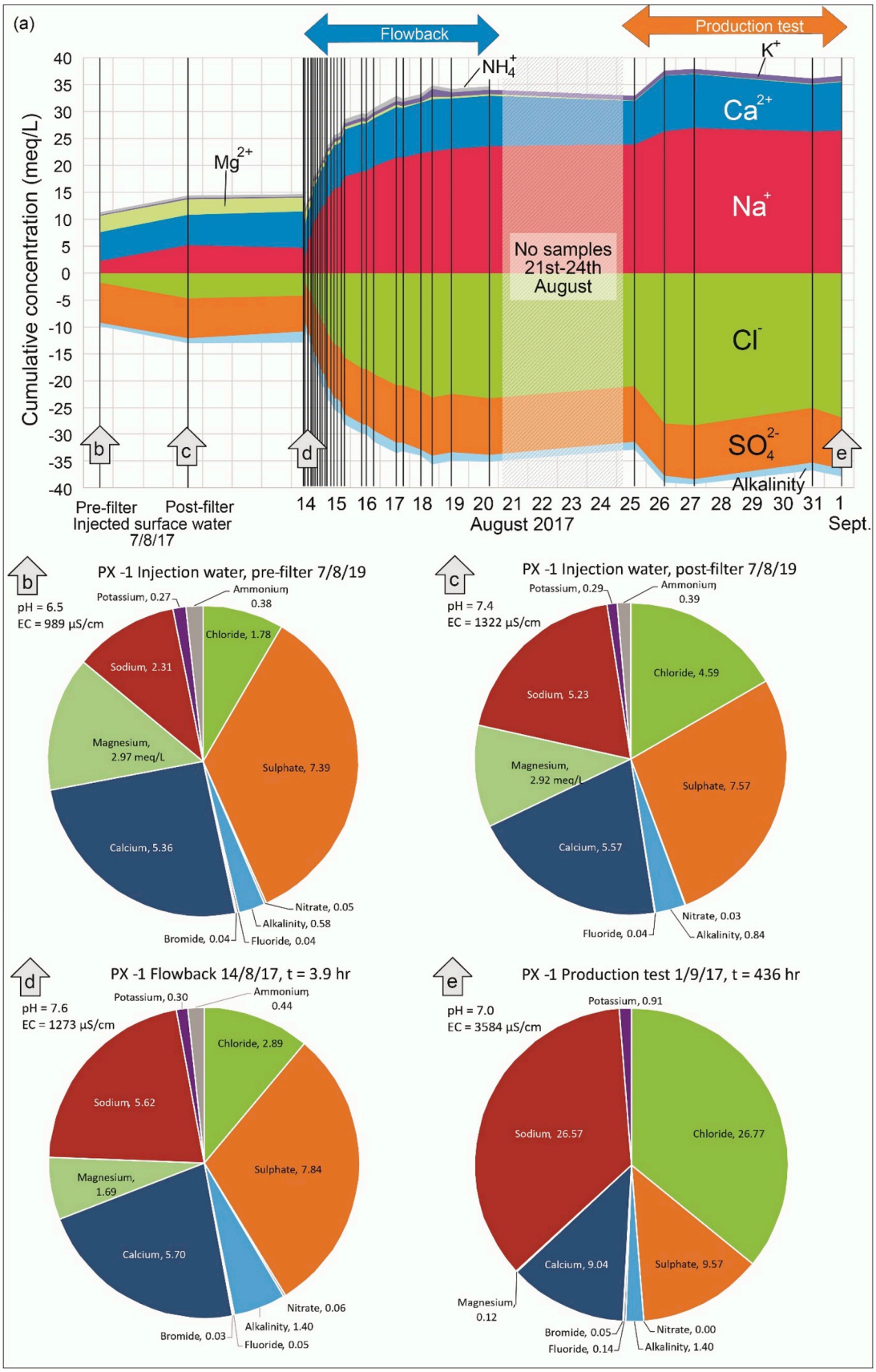

Fig. 4. (a) The evolution of flowback water hydrochemistry. Ammonium was not analysed for samples collected after 20th August. Vertical black lines show sampling events. (b–e) Pie diagrams showing the relative distributions of major cations and anions in selected water samples, in proportion to the meq/L concentrations of the ions.

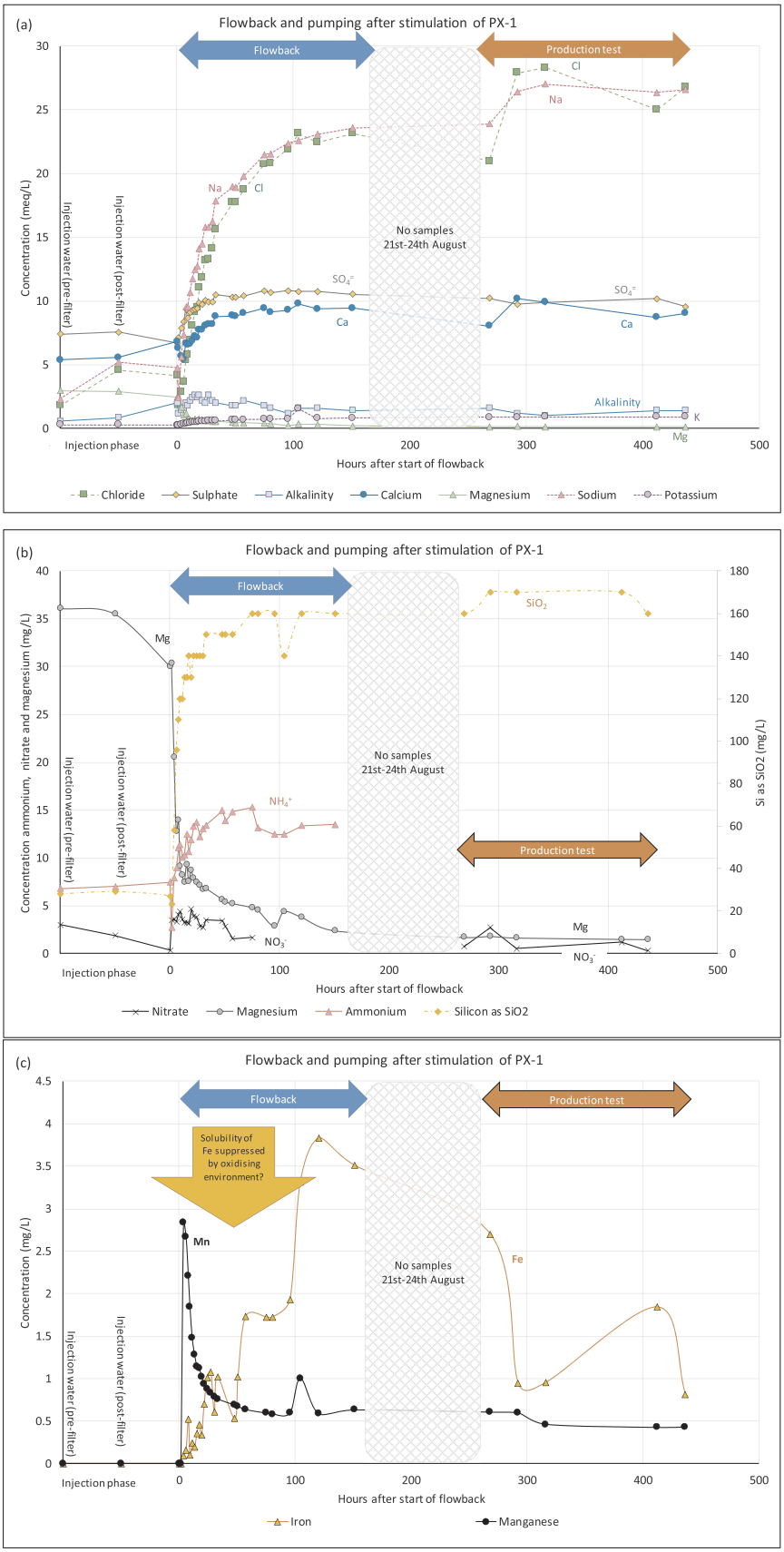

Fig. 5. (a) Concentrations of major cations and anions in flowback fluid (in meq/L) from PX-1, and water produced during production test of PX-1 in August 2017. Elapsed time is measured in hours since start of flowback (09:34 on 14th August 2017). Alkalinity effectively represents bicarbonate; (b and c) mg/L concentrations of selected minor parameters in flowback and production water.

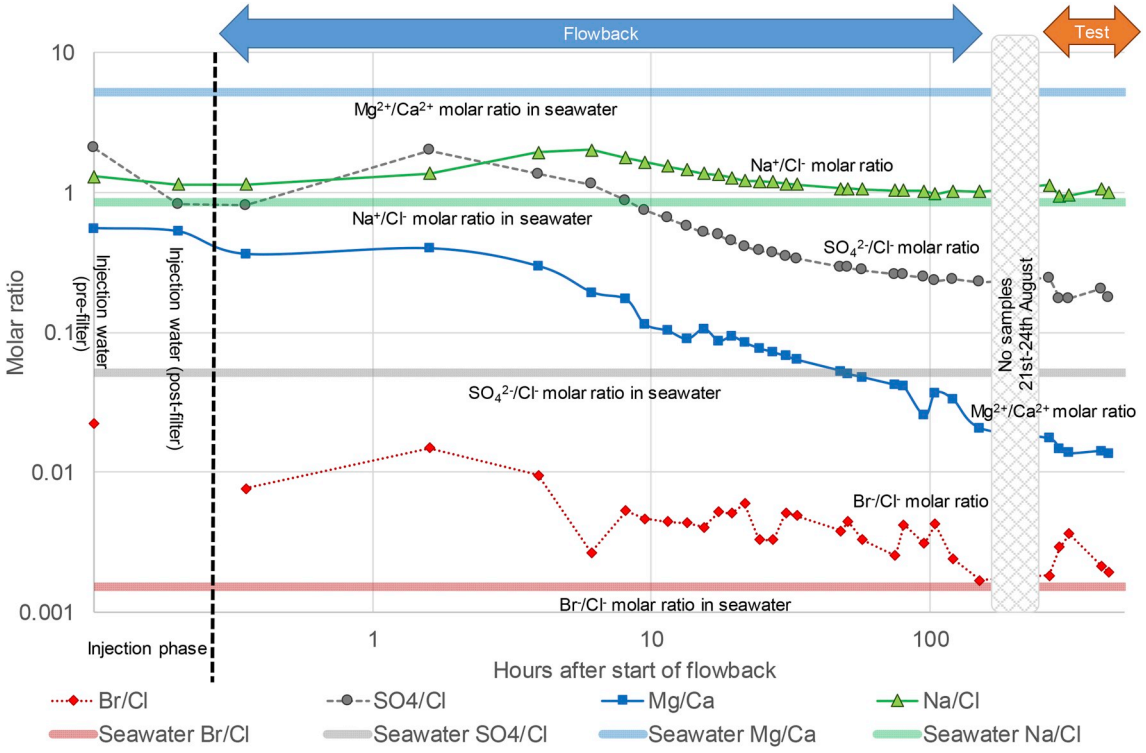

Fig. 6. Key ionic molar ratios in flowback fluid from PX-1, and water produced during production testing of PX-1 in August 2017. Seawater data after Lenntech (2019) and Stanford University (2019).

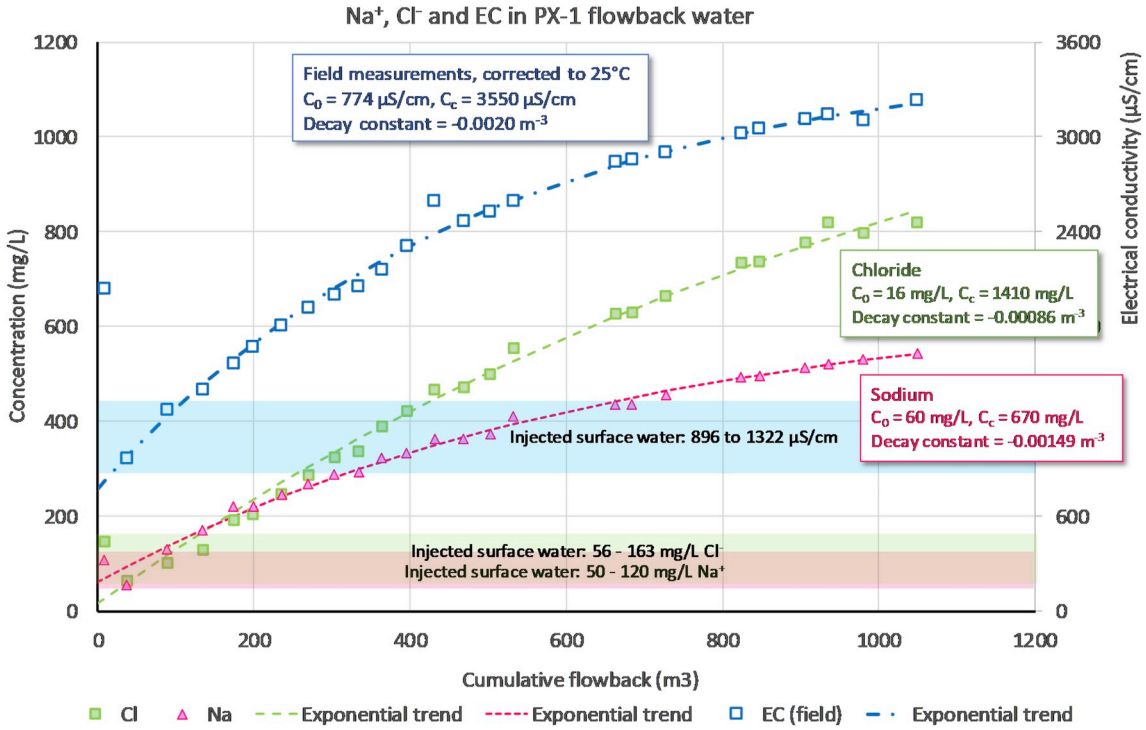

Fig. 7. Field-determined EC, and concentrations of sodium and chloride in flowback fluid from PX-1 in August 2017, plotted versus cumulative flowback following hydraulic stimulation. Sampling events are shown as symbols, while the dashed curves show best fit exponential 'flushing' curves described by Equation (1).

Thomas, 1979; Gunnlaugsson and Einarsson, 1989).

Ammonium shows a sharp increase in concentration in the flowback water, climbing to 12–15 mg/L (Fig. 5b). Nitrate shows the opposite trend, peaking shortly after commencement of flowback at almost 5 mg/L and then slowly declining to sub-mg/L values. This corresponds with evolving redox conditions in the flowback water; ORP decreases from −120 mV on 15th August (27 h) to −180 mV by 19th-20th August (120 h). Earlier flowback samples are more oxidising, being dominated by injected surface water, whilst the deep *in situ* groundwater is more reducing, with low nitrate and elevated ammonium.

This strongly suggests that, although the injected water was oxidising, any oxidising species in the water are consumed in the formation, perhaps by oxidation of sulphides or reduced iron species. This interpretation is supported by the sulphate, iron and manganese data (Fig. 5c). Injected surface water does not contain detectable dissolved Fe or Mn; however, significant concentrations (>1 mg/L) are present in flowback waters. Both these elements can be mobilised by dissolution under reducing conditions (Suter et al., 1991). Iron can also be mobilised by oxidation of pyrite, which has been observed forming fracture fill in co-magmatic granite outcrops to the north of Pohang by R.W. and G.Z. The sulphate data (Fig. 5a; 6) provides evidence of water-rock interaction releasing surplus sulphate to the flowback water.

Both Fe and Mn have "sweet" spots in terms of redox-dependent mobility – if the Eh is too high, they will be immobilised as Fe(III) or Mn(IV) oxyhydroxides; if it is too low they can be immobilised as sulphides or carbonates (Alvi and Winterhalter, 2001; Tullborg et al., 2010). Fe is typically immobilised more readily than Mn as an oxyhydroxide (Johnson, 2003; Nairn and Hedin, 1993), and this can be seen by the relative positions of the maxima of iron (120 h) and manganese (earliest samples) concentrations in Fig. 5c. In samples <120 h, it can be assumed that residual oxygen and nitrate in the injected water suppress iron mobility– indeed, this range coincides with elevated nitrate concentration in Fig. 5b.

4.3. Dissolved silicon and geothermometry

Dissolved silicon concentrations rise rapidly in recovered waters (Fig. 5b), in a manner that reflects temperature, reaching a maximum of 160–170 mg/L as SiO_2 (similar to Fig. 1) after c. 75 hrs and thereafter increasing no further. This strongly suggests that concentrations of silicon are not governed purely by a 'flushing' model, but silicon is dissolved by rapid water-rock interaction in the formation (speculatively, both quartz dissolution and silicate hydrolysis), with concentrations being limited by temperature and by silica saturation. If we assume a chalcedony control on silica concentrations, a concentration of 160–170 mg/L suggests downhole equilibration temperatures of 138–142 °C, using the geothermometer of Arnórsson et al. (1983). A quartz control would suggest temperatures of 165–169 °C (Fournier, 1977). These ranges approximately coincide with the reported temperature of 103 °C at 2250 m depth (Yoon et al., 2015), just above the top of the Pohang granodiorite, and the likely calculated temperature of 160 °C at c. 4.3 km depth (Kim and Lee, 2007).

4.4. Origin of salinity in recovered water

Fig. 6 shows key ratios between ions. The molar ratio Na^+/Cl^- increases after flowback commences, peaking after around 6 h at a value 2.02, far higher than observed in the injection water, and then gradually declines to c. 1 after 100 h. This early increase in Na^+/Cl^- is a likely indicator of water-rock interaction, with sodium (but not chloride) being released by hydrolysis of Na-silicates in the granodiorite (e.g. plagioclase, micas or amphiboles; Frengstad and Banks, 2000; Banks and Frengstad, 2006). The Br^-/Cl^- molar ratio is relatively high in the injection water (0.023) and declines over the course of the monitoring period to 0.0017. The fact that both Br^-/Cl^- and Na^+/Cl^- tend towards ratios associated with ocean water ($Br^-/Cl^- = 0.00152$, $Na^+/Cl^- = 0.86$ M ratios) strongly suggests that the salinity in the *in situ* groundwater is ultimately derived from marine salts. The *in situ* groundwater in the granodiorite (which may have been impacted by the previous stimulations) does not appear to be as saline as sea water and may thus represent a mixture between infiltrated ocean water (not unlikely given the coastal location of Pohang) and fresher onshore groundwater.

The SO_4^{2-}/Cl^- molar ratio increases following commencement of flowback, peaks at 1.6 h and thereafter gradually declines. Throughout the entire monitoring period, however, it remains substantially above the ratio observed in standard ocean water (Lenntech, 2019), further supporting the hypothesis of release of sulphate to groundwater by oxidation of sulphide minerals. It also suggests that even in the deep *in situ* groundwaters there is a sulphate excess that cannot be explained simply by present or past intrusion of marine water.

4.5. Flushing curves as identifiers of water-rock interaction

It has already been noted that the curve of electrical conductivity versus time resembles a 'flushed mixing tank' curve (Fig. 3), where one end member (injected fresh water, characterised by composition C_0) is progressively displaced by a second (*in situ* groundwater, characterised by composition C_C) in a volume (fracture systems and borehole) functioning as an idealised flushed reservoir, according to Equation (1). This type of evolution is well recognised in groundwater systems, having been especially applied to the flushing of the reaction products of pyrite oxidation from mine systems (Gzyl and Banks, 2007; Frost, 1979; Younger, 2000). However, as the flow rate for Pohang PX-1 is *not* constant, it is more appropriate to plot the concentrations of solutes against cumulative outflow from the system (flowback) rather than time. When this is done, it is found that solutes such as sodium and chloride follow ideal exponential-decay 'flushing' curves of the form of Equation (1) (Fig. 7).

Unlike sodium, which can be derived from rapid water-rock interaction in silicate lithologies (Banks et al., 1993, 1998), chloride can be regarded as a conservative tracer of flushing of the injected fresh water by *in situ* groundwater. The best fit flushing curve predicts that, eventually, the flowback water might achieve a concentration of chloride of 1410 mg/L (Fig. 7).

This chloride conservative flushing curve provides a means of identifying those solutes which are added to or removed from the system as a result of water-rock interaction. If one normalises the flushing curves in Figs. 7 and 8 by equating the lowest (initial) concentration to 0% and the highest (latest) value to 100%, one finds that other approximately conservative (in this context) solutes such as bromide, ammonium, strontium, molybdenum, boron and calcium exhibit flushing curves coincident with chloride (Fig. 8). The normalised curve for arsenic also behaves approximately coincidently with chloride, reaching maximum concentrations of over 500 μg/L. In the latest samples, however, arsenic concentrations show some signs of declining again, possibly indicating a redox control (e.g. immobilisation in a sulphide phase).

Fig. 9 applies the same methodology to sodium and potassium. The normalised flowback curves for these cations lie close to that for chloride, indicating relatively conservative behaviour. However, especially in the earlier data, the Na^+ and K^+ data lie distinctly above the chloride data, indicating a surplus concentration of both cations that cannot be explained merely by a flushing curve between two end members. This means that the flowback water has received an input of sodium and potassium during its residence in the granodiorite, most likely by hydrolysis of plagioclase, K-feldspar, micas, amphiboles or sheet silicates (as noted by Na^+/Cl^- ratios of Fig. 6).

In Fig. 10a, the technique is applied to dissolved silicon (expressed as SiO_2), temperature, barium, sulphate and magnesium. In the case of magnesium, the lowest (final) concentration is set at 100% and the maximum (early) concentration at 0%.

Temperature does not follow a conservative flushing curve (Fig. 10a). The samples (especially the early samples) contain excess heat, over and above that which can be explained by flushing in a "mixing tank environment". The excess heat is derived from water-rock interaction: conductive transfer of heat from the deep granodiorite via fracture surfaces to the injected water. The temperature declines as flowback progresses, as the declining flowback rates allow heat to be lost more effectively to the cool near surface strata during the slow ascent of water along the borehole to the surface.

Silica data approximately coincide with the temperature data, at least in the early-mid phase of the plot. This indicates, not only that

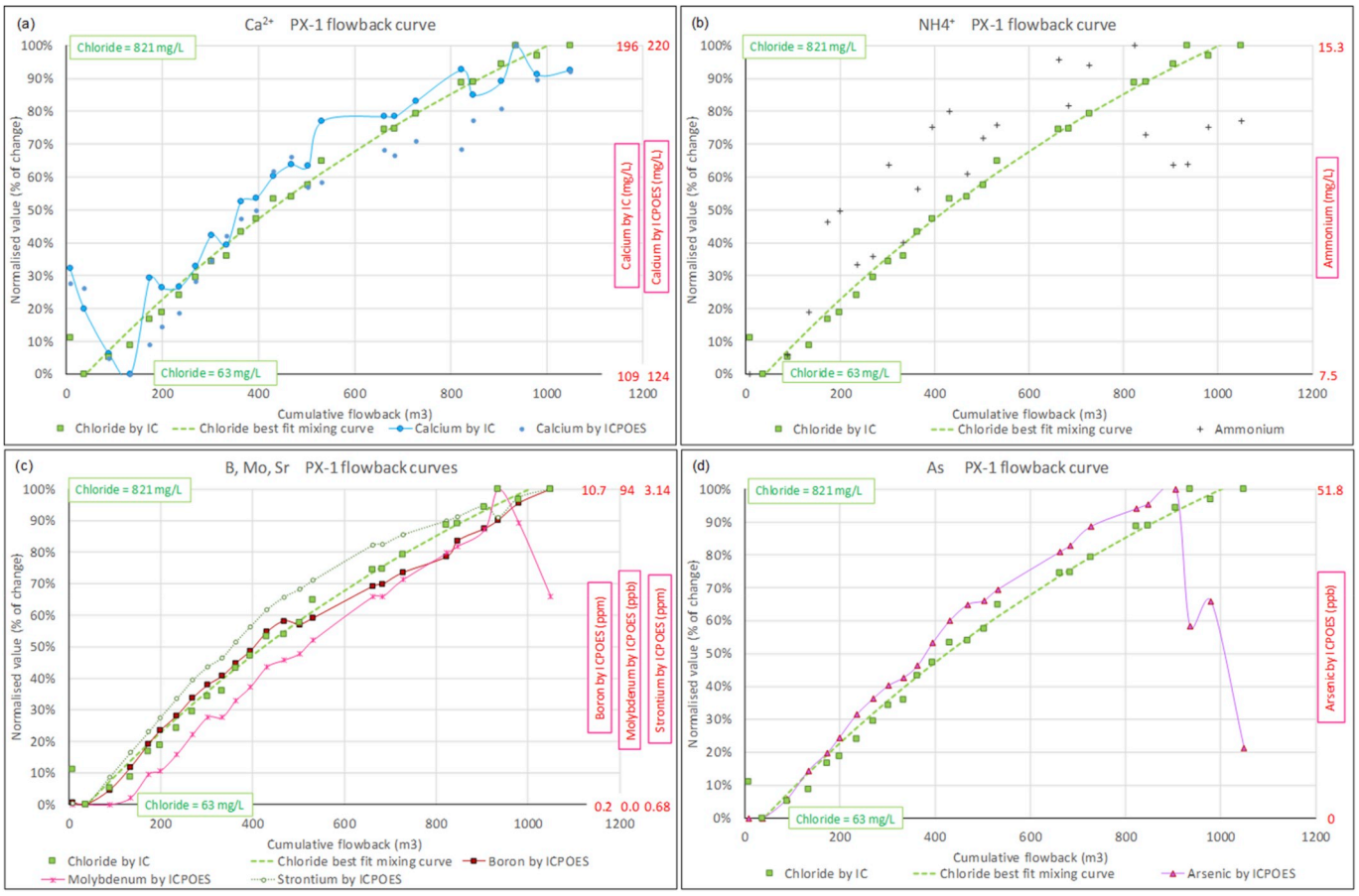

Fig. 8. Plots of (a) calcium, (b) ammonium, (c) strontium, molybdenum and boron, and (d) arsenic in flowback water from PX-1 in August 2017. In all cases, the data are normalised, with the minimum concentration being set to 0% and the maximum to 100%. The chloride data and best fit exponential flushing curve for chloride (from Fig. 7) are also shown for comparison. All these solutes exhibit approximately conservative (mixing/flushing between two end-members) behaviour.

there is a significant surplus concentration of silica, but that it is likely to be temperature-controlled. The additional silica could have been gained by the injected water from the Pohang granodiorite by quartz dissolution, and potentially additionally by hydrolysis of other silicates, such as feldspars (as evidenced by surplus Na^+ and K^+ in Fig. 9). The ability of the injected water to dissolve quartz lends support to the hypothesis of Westaway and Burnside (2019) that quartz dissolution by injected water on critically stressed fracture surfaces could lower the trigger threshold for a seismic event.

The surplus sulphate in the flowback water has already been discussed in Section 4.2, but this is also seen clearly in Fig. 10. The similarity with the normalised curve for barium, which also shows a surplus in the flowback water, is unusual. In many groundwaters, barium and sulphate exhibit an inverse relationship due to the common ion effect producing a barite ($BaSO_4$) saturation ceiling (Monnin, 1999; Appelo and Postma, 2004). However, barite solubility is temperature dependent, reaching a peak at around 100°C–160 °C, with solubility also increasing with salinity (Blount, 1977). Thus, what we could be seeing is simply barium being acquired by the flowback water as a result of elevated temperature lifting the barite solubility ceiling.

The magnesium curve (which plots a normalised *decline* in concentrations, rather than an increase), also falls dramatically above the conservative chloride flushing curve. This indicates that magnesium is being lost by water-rock interaction – potentially, by immobilisation in magnesium silicates, sheet silicates or clay minerals.

5. PHREEQC Modelling

Sample SK20 of the injection water post-filter and three selected samples of flowback water (all with low ion balance errors, namely SK25, SK33 and SK46) were simulated for major ion speciation using the programme PHREEQC Interactive (Parkhurst and Appelo, 2013). Samples were simulated at atmospheric pressure and at the pH and temperature conditions reported at the wellsite. The following parameters were used as input: alkalinity, Ba, Ca, Cl^-, K, Mg, nitrate (N(V)), ammonium (N-III), Na, sulphate (S(VI)), Si, Sr. Redox sensitive parameters were not simulated as confidence in redox quantified (dissolved oxygen, ORP, nitrate) was not sufficiently high, due to unavoidable site considerations and transport delays. Aluminosilicate minerals were not simulated as dissolved aluminium was typically at or below detection limit, as one would expect in circumneutral waters (van Helvoot et al., 2009). Samples SK33 and SK46 were re-simulated at temperature and pressure conditions plausibly representative of the downhole reservoir. Results are shown in Table 2.

The injected water was undersaturated with respect to calcite. Thus, on entering the granodiorite, alkalinity would be expected to accumulate in the water (either from calcite dissolution or silicate hydrolysis by CO_2) until calcite saturation is reached. As temperature increases, the solubility of calcite decreases, potentially resulting in a subsequent decline in alkalinity (calcite reprecipitation). This pattern of an initial increase and subsequent decrease in alkalinity is observed in Fig. 5a. Calcite is consistently close to saturation in all the flowback samples, suggesting it is the controlling factor for alkalinity.

It will be seen that both gypsum and anhydride are undersaturated in all samples. However, at conditions approximating downhole temperature and pressure, anhydride becomes saturated and could thus act as a controlling mineral phase for maximum concentrations of sulphate and calcium in *in situ* groundwater.

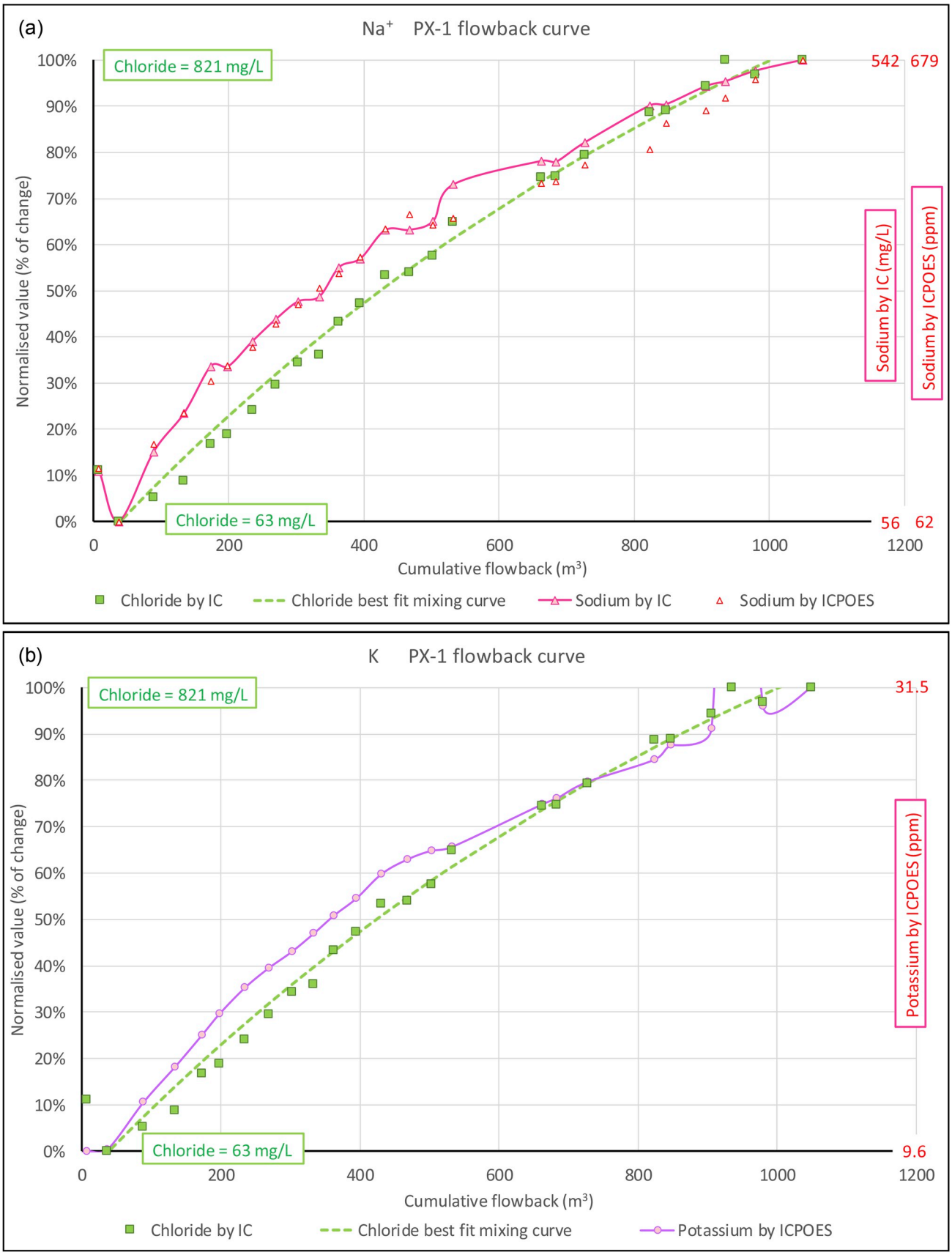

Fig. 9. Normalised plots of (a) sodium and (b) potassium in flowback water from PX-1 in August 2017. Both solutes exhibit a modest surplus concentration (above the chloride conservative flushing curve) in early data, indicative of water-rock interaction.

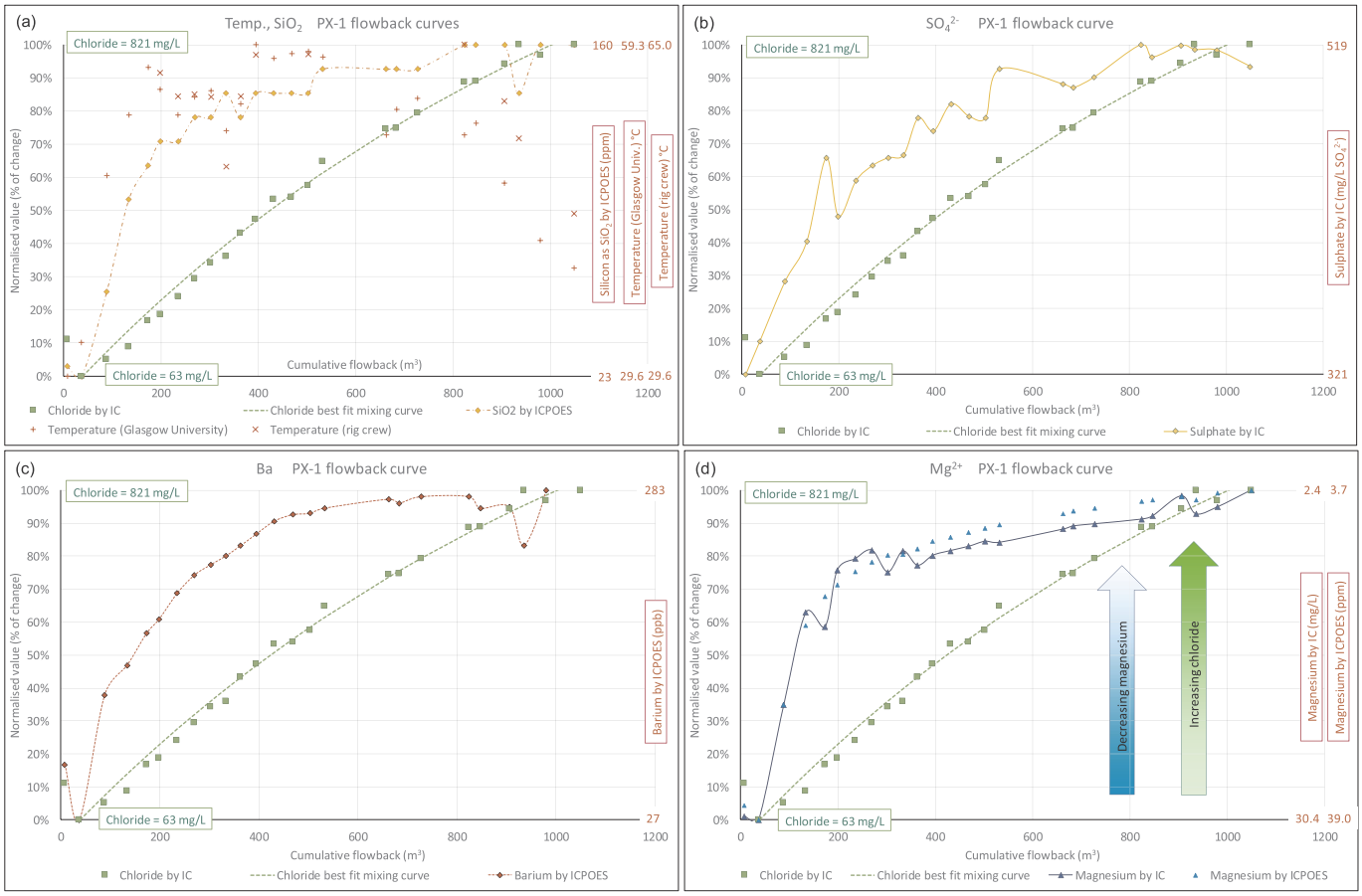

Fig. 10. Plots of (a) temperature and dissolved silicon, (b) sulphate, (c) barium, and (d) magnesium in flowback water from PX-1 in August 2017. For Mg normalisation, values are inverse, with the maximum concentration is set at 0% and the minimum at 100%.

Table 2
Results of PHREEQCI modelling of mineral saturation indices (values > 0 indicate supersaturation, <0 undersaturation) of the injection water (SK20) and three selected samples of flowback. Columns in black show modelling runs carried out at atmospheric pressure and recorded wellhead temperature. Columns with additional annotation show runs carried out applying plausible downhole conditions of 160 °C and 42.2 MPa. Arguably, the pressure could have been increased still further to account for applied injection pressures. Underlined italic text shows approximate saturation (Saturation Index <±0.5), while underlined bold text indicates significant oversaturation (>+0.5).

Sample	SK20	SK25	SK33	SK33 160 °C 42.2 MPa	SK46	SK46 160 °C 42.2 MPa
Time (hrs)	0	6.10	21.7		151.3	
Cumulative flowback (m^3)	0	130	421		821	
pH (field)	7.4	7.35	6.86	6.86	7.23	7.23
Temperature (°C)	29.5	53.0	63.9	160	47.0	160
Anhydrite [$CaSO_4$]	−1.29	−1.00	−0.75	*+0.21*	−0.89	*+0.26*
Aragonite [$CaCO_3$]	−0.54	*−0.03*	*−0.15*	**+0.72**	*−0.14*	**+0.70**
Barite [$BaSO_4$]	*+0.23*	*+0.50*	**+0.63**	*+0.21*	**+0.93**	*+0.49*
Calcite [$CaCO_3$]	*−0.40*	*+0.09*	*−0.03*	**+0.79**	*−0.01*	**+0.76**
Celestite [$SrSO_4$]	−1.43	−1.16	−0.86	−0.86	−0.78	−0.51
Chalcedony [SiO_2]	*−0.13*	*+0.13*	*+0.19*	−0.57	*+0.41*	−0.51
Chrysotile [$Mg_3Si_2O_5(OH)_4$]	−4.01	−2.26	−4.59	**+2.23**	−5.46	**+2.92**
Dolomite [$CaMg(CO_3)_2$]	−0.92	*−0.31*	−0.94	−1.25	−1.46	−1.91
Gypsum [$CaSO_4.2H_2O$]	−1.03	−0.98	−0.84	−0.61	−0.81	−0.57
Quartz [SiO_2]	*+0.28*	*+0.48*	**+0.51**	*−0.43*	**+0.78**	*−0.37*
Sepiolite [$Mg_2Si_3O_7(OH)_5.3H_2O$]	−3.27	−2.46	−4.25	−2.81	−3.92	−2.26
Strontianite [$SrCO_3$]	−2.13	−1.57	−1.59	−1.30	−1.43	−1.02
Talc [$Mg_3Si_4O_{10}(OH)_2$]	−4.30	**+2.03**	*−0.08*	**+5.99**	−0.66	**+6.79**

Barite is slightly oversaturated in the injection water and its oversaturation increases with flowback. However, at downhole temperature and pressure, its saturation index decreases dramatically, illustrating the sensitivity of barite solubility to both temperature and pressure (Blount, 1977). The excess barium concentrations seen in Fig. 10 could thus be due to the effect of downhole temperature and high applied injection pressures (in excess of those modelled in Table 2) increasing barite solubility and effectively causing pressure solution of barite, without the solution re-equilibrating on transit to the surface.

Finally, PHREEQCI modelling illustrates that there are plausible sinks for magnesium via water-rock interaction: for example, the minerals talc ($Mg_3Si_4O_{10}(OH)_2$) and chrysotile ($Mg_3Si_2O_5(OH)_4$) become

significantly oversaturated under conditions of high temperature and pressure. There are a number of other, arguably more plausible, magnesium aluminosilicates (e.g. stevensite and smectite; Kasai et al., 2000), which cannot be modelled, due to lack of dissolved Al data, that could also be candidate sinks for magnesium in the geothermal reservoir.

6. Conclusions

Hydrochemical analysis of flowback water from the 4.3 km deep Pohang PX-1 well provides insights into water-rock interactions during a controlled granodiorite hydraulic stimulation. The injected surface water was a relatively fresh, oxidising, calcite-undersaturated, circumneutral calcium-sulphate water derived from an irrigation pond near the borehole site. Flowback water temperature peaked at 65 °C after 75 h and then declined, as a result of slower fluid ascent allowing greater loss of heat to shallow near-surface strata. Quartz (169 °C) and chalcedony (142 °C) geothermometers are consistent with independent downhole measurements and reservoir temperature estimates based on measured geothermal gradients. $\delta^{18}O$ and $\delta^{2}H$ data show a clear trajectory from the injected surface water, which displays a mild evaporative signal, to the last samples of produced *in situ* groundwater, which has undergone oxygen isotope exchange with the mineral matrix at high temperature.

As flowback progressed, produced water evolved to a brackish (EC at 25 °C = c. 3200 μS/cm) sodium chloride, calcite-saturated reducing composition. The *in situ* redox condition is iron-, manganese-, and nitrate-reducing, and around the sulphate-reduction threshold. The *in situ* groundwater contains significant sulphate concentrations (>500 mg/L), but there is also evidence that injection of surface water caused further oxidation of sulphide minerals. Na^{+}/Cl^{-} and Br^{-}/Cl^{-} ratios evolved towards values consistent with a marine origin for salinity, but as *in situ* groundwater is not highly saline, we infer it to be a mixture between fresh groundwater and marine intrusion (possibly also modified by previous stimulations).

Chloride concentrations evolve as an exponential flushing curve when plotted against cumulative flowback. This indicates that the injected fresh water was progressively flushed out during flowback in a mixing-tank-like environment (representing the fracture network and borehole) by the *in situ* groundwater. This conservative 'flushed mixing tank' model suggests that the true *in situ* groundwater in the granodiorite might exhibit chloride concentrations as high as 1410 mg/L and electrical conductivity as high as 3600 μS/cm. Like chloride, normalised concentrations of most other solutes (ammonium, arsenic, boron, bromide, calcium, molybdenum and strontium) exhibit quasi-conservative behaviour. Sodium and potassium initially exhibit slight excess concentrations, suggesting hydrolysis of silicate minerals.

Sulphate and barium exhibit significant excess concentrations in flowback. Sulphate is likely derived from sulphide oxidation by injected water, while PHREEQCI modelling tentatively suggests that barium may be derived from pressure solution of barite at high downhole temperatures. Silicon also exhibits surplus concentrations, which follow a similar pattern to temperature and strongly suggests dissolution of quartz at elevated downhole temperatures, probably supplemented by aluminosilicate hydrolysis. This lends tentative support to the hypothesis of Westaway and Burnside (2019) that quartz dissolution by injected water on critically stressed fault planes could affect frictional resistance to slip and facilitate seismicity.

Our assessment demonstrates the value of continued hydrochemical monitoring and analysis throughout geothermal project-related activities. Clear trends in the evolutions of physicochemical and isotopic parameters throughout the August 2017 hydraulic stimulation at the Pohang EGS site provide several indicators of water-rock interaction. Some of these could either aid or hinder operational EGS performance and could have potentially influenced local seismic events. However, the lack of hydrochemical data from previous and subsequent stimulations make it difficult to perform a full assessment of this aspect. From interpretation of the data that do exist, we can make some broad recommendations to diminish risk of unintended water-rock interaction at any geothermal project that seeks to inject non-*in situ*-equilibrated waters. First, perform robust baseline analysis of hydrochemical characteristics within target reservoirs prior to any major activity. Second, carry out regular physicochemical monitoring of injected water, flowback and produced water for temperature, pH, EC, redox potential, major ions, silicon and other key hydrochemical indicators. Third, consider appropriate sources of - or additives to - injected waters to avoid any problematic water-rock interactions for system performance - for example, injection of warm, silica-saturated water, rather than cold, silica undersaturated water.

Declaration of competing interest

The authors declare that they have no known competing financial interests or personal relationships that could have appeared to influence the work reported in this paper.

Acknowledgements

This work was funded by the European Commission Horizon 2020 LCE 'DESTRESS' project (EC-691728). AJB was funded by, and isotopic analyses carried out at, the ICSF at SUERC (NERC Facility contract F14/G6/11/01). We thank: NexGeo for access to the Pohang site for sampling; Anne McGarrity and Alison McDonald for analyses; Eunhyea Chung and Ki-Bok Min, and their respective teams, of Seoul National University for collecting samples and providing additional data; and many DESTRESS co-workers for helpful discussions. We especially thank Paul Younger (deceased 21 April 2018), who led UoG involvement in DESTRESS and helped to secure the funding for this work.

Appendix. Supplementary data

Supplementary data to this article can be found online at https://doi.org/10.1016/j.apgeochem.2019.104445.

References

Alvi, K., Winterhalter, B., 2001. Authigenic mineralisation in the temporally anoxic Gotland deep, the Baltic sea. Baltica 14, 74–83.
Appelo, C., Postma, D., 2004. Geochemistry, Groundwater and Pollution, second ed. CRC Press, London, p. 678.
Arnórsson, S., Gunnlaugsson, E., Svavarsson, H., 1983. The chemistry of geothermal waters in Iceland. III. Chemical geothermometry in geothermal investigations. Geochem. Cosmochim. Acta 47 (3), 567–577.
Banks, D., Brehme, M., 2017. Geochemistry and hydrochemistry (DESTRESS best practice guide). Available Online. http://www.destress-h2020.eu/en/Best-Practices/Geochemistry-and-Hydrochemistry/. (Accessed 27 October 2018).
Banks, D., Frengstad, F., 2006. Evolution of groundwater chemical composition by plagioclase hydrolysis in Norwegian anorthosites. Geochem. Cosmochim. Acta 70, 1337–1355.
Banks, D., Rohr-Torp, E., Skarphagen, H., 1993. Groundwater chemistry in a Precambrian granite island aquifer, Hvaler, Southeastern Norway. In: Hydrogeology of Hard Rocks, Mem. 24th Congress of International Association of Hydrogeologists, 28th June- 2nd July 1993, Ås (Oslo), Norway, 1993.
Banks, D., Frengstad, B., Midtgård, A., Krog, J., Strand, T., 1998. The chemistry of Norwegian groundwaters: I. The Distribution of Radon, Major and Minor elements in 1604 crystalline bedrock groundwaters. Sci. Total Environ. 222, 71–91.
Banks, D., Burnside, N.M., Westaway, R., Zimmermann, G., Hofmann, H., 2019. Exponential trends in flowback chemistry from a hydraulically stimulated deep geothermal borehole in granite; Pohang, South Korea. In: Proc. 16th International Symposium on Water-Rock Interaction and 13th International Symposium on Applied Isotope Geochemistry (1st IAGC International Conference), July 21-26, 2019, Tomsk, Russia, Tomsk, Russia.
Bartram, J., Ballance, R., 1996. Water Quality Monitoring: a Practical Guide to the Design and Implementation of Freshwater Quality Studies and Monitoring Programs. E & FN Spon on behalf of United Nations Environment Programme and the World Health Organization, London.
Blattner, P., 1985. Isotope shift data and the natural evolution of geothermal systems. Chem. Geol. 49, 187–203.
Blount, C., 1977. Barite solubilities and thermodynamic quantities up to 300°C and 1400 bars. Am. Mineral. 62, 942–957.

Burnside, N.M., Banks, D., Boyce, A., 2016. Sustainability of thermal energy production at the flooded mine workings of the former Cap house Colliery, Yorkshire, United Kingdom. Int. J. Coal Geol. 164, 85–91.
Clayton, R.N., Steiner, A.S., 1975. Oxygen isotope studies of the geothermal system at Wairakei, New Zealand. Geochem. Cosmochim. Acta 39, 1179–1186.
Cox, M., Thomas, D., 1979. Chloride/Magnesium Ratio of Shallow Groundwaters as a Regional Geothermal Indicator in Hawaii. Hawaii Institute of Geophysics Report HIG-79-9.
Davis, S., Whittemore, D., Fabryka-Martin, J., 1998. Uses of chloride/bromide ratios in studies of potable water. Gr. Water 36, 338–350.
Fournier, R., 1977. Chemical geothermometers and mixing models for geothermal systems. Geothermics 5, 41–50.
Frengstad, B., Banks, D., 2000. Evolution of high-pH Na-HCO3 groundwaters in anorthosites: silicate weathering or cation exchange?. In: Groundwater: Past Achievements and Future Challenges, Proc. XXXIInd Congress of the International Association of Hydrogeologists, Cape Town, South Africa.
Frost, R., 1979. Evaluation of the rate of decrease in the iron content of water pumped from a flooded shaft mine in County Durham, England. J. Hydrol. 40, 101–111.
Gendenjamts, O.-E., 2003. Interpretation of Chemical Composition of Geothermal Fluids from Árskógsströnd, Dalvík and Hrísey, N. Iceland and in the Khangai Area, Mongolia. United Nations University, Reykjavík, Iceland. Geothermal Training Programme. Report 2003, No. 10.
Grigoli, F., Cesca, S., Rinaldi, A., Manconi, A., López-Comino, J., Clinton, J., Westaway, R., Cauzzi, C., Dahm, T., Wiemer, S., 2018. The November 2017 Mw 5.5 Pohang earthquake: a possible case of induced seismicity in South Korea. Science 360 (6392), 1003–1006.
Gunnlaugsson, E., Einarsson, A., 1989. Magnesium-silicate scaling in mixture of geothermal water and deaerated fresh water in a district heating system. Geothermics 18 (1–2), 113–120.
Gunnlaugsson, E., Ármannsson, H., Thorhallsson, S., Steingrímsson, B., 2014. Problems in geothermal operation: scaling and corrosion. In: Proceedings "Short Course VI on Utilization of Low- and Medium-Enthalpy Geothermal Resources and Financial Aspects of Utilisation", Santa Tecla, El Salvador, 23-29 March 2014, Santa Tecla, El Salvador.
Gzyl, G., Banks, D., 2007. Verification of the "first flush" phenomenon in mine water from coal mines in the upper Silesian coal basin, Poland. J. Contam. Hydrol. 92, 66–86.
Hofmann, H., Zimmermann, G., Farkas, M., Huenges, E., Zang, A., Leonhardt, M., Kwiatek, G., Martinez-Garzon, P., Bohnhoff, M., Min, K., Fokker, P., Westaway, R., Bethmann, F., Meier, P., Yoon, K., Choi, J., Lee, T., Kim, K., 2019. First field application of cyclic soft stimulation at the Pohang enhanced geothermal system site in Korea. Geophys. J. Int. 217 (2), 926–949.
IAEA/WMO, 2018. Global network of isotopes in precipitation. The GNIP database. Available Online. https://nucleus.iaea.org/wiser. (Accessed 31 October 2018).
Johnson, K., 2003. The importance of aeration in passive treatment schemes for manganese removal. Land Contam. Reclam. 11 (2), 205–212.
Kasai, K., Sato, K., Kimura, S., Shakunaga, N., Obara, K., 2000. Characterization of smectite scale and scale inhibition test by pH control at the Mori geothermal power plant, Japan. In: Proceedings of the World Geothermal Congress 2000, Kyushu-Tohoku, Japan, May 28 - June 10, 2000. Kyushu-Tohoku, Japan.
Kim, H., Lee, Y., 2007. Heat flow in the Republic of Korea. J. Geophys. Res. 112, B05413.
Kim, K.-H., Ree, J.-H., Kim, Y.-H., Kim, S., Kang, S.-Y., Seo, W., 2018. Assessing whether the 2017 Mw 5.4 Pohang earthquake in South Korea was an induced event. Science 360 (6392), 1007–1009.
KMA (Korea Meteorological Administration), 2016. Pohang, geography and climate. Cited on Wikipedia. Available Online. https://en.wikipedia.org/wiki/Pohang. (Accessed 31 October 2018).
Lee, K., 2017. Hankyoreh online: scientists discuss correlation between geothermal plant and Pohang earthquake 27/11/2017. Available Online. http://english.hani.co.kr/arti/english_edition/e_national/820906.html. (Accessed 14 February 2018).
Lee, S., Kim, T., Lee, T., 2011. Strontium isotope geochemistry and its geochemical implication from hot spring waters in South Korea. J. Volcanol. Geotherm. Res. 208, 12–22.
Lee, T.-H., Yi, K., Cheong, C.-S., Jeong, Y.-J., Kim, N., Kim, M., 2014. SHRIMP U-Pb zircon geochronology and geochemistry of drill cores from the Pohang basin. J. Petrol. Soc. Korea 23 (3), 167–185.
Lee, T., Song, Y., Park, D.-W., Jeon, J., Yoon, W., 2015. Three-dimensional geological model of Pohang EGS pilot site, Korea. In: Proceedings of the World Geothermal Congress, Melbourne, Australia, 19-25 April 2015.
Lee, K.-K., Yeo, I.-W., Lee, J.-Y., Kang, T.-S., Rhie, J., Sheen, D.-H., Chang, C., Son, M., Cho, I.-K., Oh, S., Pyun, S., Kim, S., Ge, S., Ellsworth, W., Giardini, D., Townend, J., Shimamoto, T., 2019. Summary Report of the Korean Government Commission on Relations between the 2017 Pohang Earthquake and the EGS Project. Geological Society of Korea and Korean Government Commission on the Cause of the Pohang Earthquake, Seoul, Republic of Korea.
Lenntech, 2019. Composition of seawater. Available Online. https://www.lenntech.com/composition-seawater.html. (Accessed 11 April 2019).
Misstear, B., Banks, D., Clark, L., 2017. Water Wells and Boreholes, second ed. John Wiley & Sons Ltd, Chichester.
Monnin, C., 1999. A thermodynamic model for the solubility of barite and celestite in electrolyte solutions and seawater to 200°C and to 1 kbar. Chem. Geol. 153 (1), 187–209.
Nairn, B., Hedin, R., 1993. Contaminant removal capabilities of wetlands constructed to treat coal mine drainage. In: Constructed Wetlands for Water Quality Improvement. Lewis/CRC Press, Boca Raton, USA, pp. 187–195.
Park, J.-Y., Kim, J.-M., Yoon, S.-H., 2015. Three-dimensional geologic modeling of the Pohang Basin in Korea for geologic storage of carbon dioxide. J. Geol. Soc. Korea 51 (3), 289–302.
Park, S., Xie, L., Kim, K.-I., Kwon, S., Min, K.-B., Choi, J., Yoon, W.-S., Song, Y., 2017. First hydraulic stimulation in fractured geothermal reservoir. Procedia Eng. 191, 829–837.
Parkhurst, D., Appelo, C., 2013. Description of input and examples for PHREEQC version 3: a computer program for speciation, batch-reaction, one-dimensional transport, and inverse geochemical calculations. In: U.S. Geological Survey Techniques and Methods, Book 6. United States Geological Survey, Denver, Colorado, p. 497. Chapter A43.
Rimstidt, J., Barnes, H., 1980. The kinetics of silica-water reactions. Geochem. Cosmochim. Acta 44 (11), 1683–1699.
Stanford University, 2019. Mineral makeup of seawater. Available Online. https://web.stanford.edu/group/Urchin/mineral.html. (Accessed 12 April 2019).
Suter, D., Banwart, S., Stumm, W., 1991. Dissolution of hydrous iron(III) oxides by reductive mechanisms. Langmuir 7 (4), 809–813.
Tullborg, E., Smellie, J., Nilsson, A., Gimeno, M., Brüchert, V., Molinero, J., 2010. SR-site – Sulphide Content in the Groundwater at Forsmark. Svensk Kärnbränslehantering AB, Stockholm. Technical Report TR-10-39.
van Helvoort, P., Griffioen, J., Edmunds, W., 2009. Occurrence and behaviour of main inorganic pollutants in European groundwater. In: Groundwater Monitoring. John Wiley & Sons Ltd., Chichester, pp. 83–110.
Westaway, R., Burnside, N.M., 2019. Fault 'corrosion' by Fluid Injection: Potential Cause of the November 2017 Mw 5.5 Korean Earthquake, p. 23. Geofluids Article ID 1280721.
Wood, W., Sanford, W., 2007. Atmospheric bromine flux from the coastal Abu Dhabi sabkha: a ground-water mass balance investigation. Geophys. Res. Lett. 34, L14405.
Yoon, K.-S., Jeon, J.-S., Hong, H.-K., Kim, H.-G., Hakan, A., Park, J.-H., Yoon, W.-S., 2015. Deep drilling experience for Pohang enhanced geothermal project in Korea. In: Proceedings World Geothermal Congress, Melbourne, Australia, 19-25 April 2015, Melbourne, Australia.
Younger, P., 2000. Predicting temporal changes in total iron concentrations in groundwaters flowing from abandoned deep mines: a first approximation. J. Contam. Hydrol. 44, 47–69.
Yum, B., 1999. Historical review of hot spring waters in the Republic of Korea. In: Stories from a Heated Earth: Our Geological Heritage. Geothermal Resources Council, Davis, CA, USA, pp. 379–392.
Zastrow, M., 2019. South Korea accepts geothermal plant probably caused destructive quake. Nature News 22/3/2019. Available Online. https://www.nature.com/articles/d41586-019-00959-4. (Accessed 4 April 2019).